

Active oscillatory associative memory

Matthew Du,^{1,2} Agnish Kumar Behera,¹ and Suriyanarayanan Vaikuntanathan^{1,2}

¹*Department of Chemistry, University of Chicago, Chicago, Illinois 60637, USA*

²*The James Franck Institute, University of Chicago, Chicago, Illinois 60637, USA*

(Dated: July 26, 2023)

Traditionally, physical models of associative memory assume conditions of equilibrium. Here, we consider a prototypical oscillator model of associative memory and study how active noise sources that drive the system out of equilibrium, as well as nonlinearities in the interactions between the oscillators, affect the associative memory properties of the system. Our simulations show that pattern retrieval under active noise is more robust to the number of learned patterns and noise intensity than under passive noise. To understand this phenomenon, we analytically derive an effective energy correction due to the temporal correlations of active noise in the limit of short correlation decay time. We find that active noise deepens the energy wells corresponding to the patterns by strengthening the oscillator couplings, where the more nonlinear interactions are preferentially enhanced. Using replica theory, we demonstrate qualitative agreement between this effective picture and the retrieval simulations. Our work suggests that nonlinearity in the oscillator couplings can improve memory under nonequilibrium conditions.

An essential feature of biological organisms is memory, which involves the learning and retrieval of information. The importance of this cognitive ability has prompted many studies of memory from a physics perspective [1, 2], specifically associative, or content-addressable, memory [3–6].

A well explored model of associative memory is the Hopfield neural network [7], which resembles a fully connected Ising model with nonuniform and random interaction strengths. The neurons are modeled as spins and the learned patterns, which are drawn from a probability distribution, are encoded in the couplings between spins. Naturally, the memory capabilities of the Hopfield model can be understood from the perspective of statistical mechanics [8–11]. Refs. [8–10] showed that thermal fluctuations in the firing rates of neurons leads to poorer recall of patterns.

However, it is unclear whether such findings, which characterize the system at equilibrium, apply to biological systems which are expected to be subjected to noise sources that do not satisfy the constraints of equilibrium. Indeed, a proper physical description of living systems requires nonequilibrium aspects [12, 13]. Notably, the flocking of birds [14, 15] and the dynamics of the cytoskeleton [16, 17] are modeled as active matter [18–20], particles that consume energy from the environment to power their movement. Some active materials, e.g., epithelial cells [21] and colloids in a bacterial solution [22], can be described as particles subjected to so-called active noise [23, 24], which has temporal correlations (i.e., is colored noise) and does not obey detailed balance with respect to the damping. In fact, the membrane potential of neurons can have temporally correlated fluctuations [25, 26].

Additionally, a feature that the Hopfield model does not exhibit is the oscillatory activity of neurons [27–29]. This motivation led to variants [30–36] of the Kuramoto model [37] of nonlinearly coupled oscillators, whose Hopfield-like interactions give rise to associative

memory. These analog systems, due to their simplicity, can be studied in much detail using analytical methods [31, 32, 36].

Here, we study an oscillatory Hopfield network in the presence of active noise. Inspired by the Kuramoto-type models of [32, 38], the system here has not been studied before, to the best of our knowledge, even in the absence of noise. Our numerical simulations reveal that the recall of information is enhanced under active noise, relative to under comparable equilibrium conditions. We then analytically derive, in a perturbative limit, an effective energy correction associated with the temporal correlations of active noise [23, 39–41]. Using replica theory [42], we find that the effective picture describes qualitatively the improvement of associative memory under active noise. Our work sheds light on how nonlinearity in the neuron couplings impacts memory under nonequilibrium conditions.

The paper is structured as follows. We introduce the Kuramoto-type Hopfield model in Sec. I. Then, we numerically simulate pattern retrieval in Sec. II. Sec. III describes the theoretical analysis, in which we derive the effective Hamiltonian (Sec. III A) and apply replica theory to it (Sec. III B). We conclude in Sec. IV.

I. MODEL

We consider N periodic oscillators whose interactions endow the system with associative memory (Fig. 1a). Specifically, we focus on the Hamiltonian

$$H = -\frac{1}{2N} \sum_{\mu=1}^p \sum_{i,j=1}^N \xi_i^\mu \xi_j^\mu \cos \theta_i \cos \theta_j - \frac{\epsilon}{4N} \sum_{i,j=1}^N \cos 2\theta_i \cos 2\theta_j, \quad (1)$$

where $\theta_1, \dots, \theta_N$ are the oscillator phases. Analogous in form to the Hamiltonian of [38], H is a generalization of the Kuramoto model [37] that features associative memory. Collectively, the phases and their cosines will be referred to as $\boldsymbol{\theta} = (\theta_1, \dots, \theta_N)$ and $\mathbf{c}(\boldsymbol{\theta}) = (\cos \theta_1, \dots, \cos \theta_N)$, respectively.

The first term of H encodes p patterns (Fig. 1b) $\boldsymbol{\xi}^1, \dots, \boldsymbol{\xi}^p \in \{\pm 1\}^N$ learned by the Hebb rule [7, 43]. Appearing in the model of Ref. [32], this term is analogous to the Hopfield Hamiltonian [7], where the variable of spin i is replaced by $\cos \theta_i$ and the couplings are of the form $\cos \theta_i \cos \theta_j$. All pattern elements are independent and identically distributed (i.i.d.) random variables drawn uniformly from $\{\pm 1\}$ (i.e., a binomial distribution). When the pattern loading $\alpha = p/N$ is sufficiently small, the system has energy minima near the pattern configurations (Fig. 1c) $\{\boldsymbol{\theta}^{\boldsymbol{\xi}^\mu}\}_{\mu=1}^p$, where $\mathbf{c}(\boldsymbol{\theta}^{\boldsymbol{\xi}^\mu}) = \boldsymbol{\xi}^\mu$. Henceforth, we will sometimes write “pattern” as shorthand for “pattern configuration.”

The second term of H enhances the stability of the learned patterns, as well as all other patterns, whose configurations also satisfy $\mathbf{c}(\boldsymbol{\theta}) \in \{\pm 1\}^N$. Characterized by strength ϵ , this term has couplings of the form $\cos 2\theta_i \cos 2\theta_j = (2 \cos^2 \theta_i - 1)(2 \cos^2 \theta_j - 1)$, making it more nonlinear than the pattern-encoding term. By varying ϵ in our calculations below, we can understand how nonlinearity affects memory in the presence of noise. We will restrict ourselves to intermediate values of ϵ , as the learned patterns are further stabilized (compared to $\epsilon = 0$) while the patterns that have not been learned remain relatively unstable [38].

In pattern retrieval, the system starts near a pattern $\boldsymbol{\xi} \in \{\pm 1\}^N$ and then moves towards it (Fig. 1d). The initial position is $\boldsymbol{\theta}(0) = \boldsymbol{\theta}^\xi + \boldsymbol{\delta}$, where $\mathbf{c}(\boldsymbol{\theta}^\xi) = \boldsymbol{\xi}$, $\boldsymbol{\delta}$ is a vector of N i.i.d. random variables drawn from $\mathcal{N}(0, \sigma^2)$, and σ determines the typical size of the initial offset. To represent neurons isolated from external forces, one would evolve the system via gradient descent on the energy landscape of Hamiltonian (1). However, real neurons reside in a biological environment, which can induce nonequilibrium fluctuations in the firing rates. Thus, we evolve the system according to the dynamics of active Ornstein-Uhlenbeck particles [23, 24]:

$$\frac{d\boldsymbol{\theta}}{dt} = -\nabla_{\boldsymbol{\theta}} H + \boldsymbol{\eta}(t). \quad (2)$$

The noise $\boldsymbol{\eta}$ is a stationary Gaussian process that satisfies

$$\langle \eta_i(t) \rangle = 0, \quad (3)$$

$$\langle \eta_i(t) \eta_j(t') \rangle = \frac{T}{\tau} \delta_{ij} e^{-|t-t'|/\tau}, \quad (4)$$

where the temporal correlations exponentially decay with persistence time τ and initial value T/τ . For $\tau > 0$, the noise is active, and the system is kept out of equilibrium. In the limit $\tau \rightarrow 0$, the temporal correlations satisfy

$$\lim_{\tau \rightarrow 0} \langle \eta_i(t) \eta_j(t') \rangle = 2T \delta_{ij} \delta(t-t'), \quad (5)$$

corresponding to thermal noise which drives the system towards equilibrium with temperature T . Hereafter, we refer to this type of noise as passive. To characterize the proximity of the system to $\boldsymbol{\xi}$, the order parameter that we use is the overlap $\frac{1}{N} [\boldsymbol{\xi} \cdot \mathbf{c}(\boldsymbol{\theta})]$, which ranges from 0 (farthest from pattern) to 1 (at pattern). After the system has evolved for a long time, the overlap indicates the accuracy with which the pattern has been retrieved.

II. SIMULATIONS

We simulate pattern retrieval for a system with $N = 200$ oscillators. Without loss of generality, we consider the retrieval of learned pattern $\mu = 1$ ($\boldsymbol{\xi}^1$), hereafter referred to as “target pattern.” We choose $\sigma = 0.1$, for which the typical initial overlap with the target pattern is ≈ 0.995 . The system is evolved from $t = 0$ to $t = 800$ by numerically integrating equation of motion (2) using a time step of $\Delta t = 0.004$. Below, the simulation results represent an average over 16 pattern sets and 8 initial configurations. These numbers are high enough such that the error due to finite sampling can be neglected.

We first focus on the system with just the pattern-encoding term, i.e., with $\epsilon = 0$ (Fig. 2a). In the absence of noise ($T = 0$), the learned patterns can be retrieved at higher pattern loading (α) compared to the Hopfield model, for which retrieval fails at $\alpha \gtrsim 0.138$ [8, 9]. However, the critical pattern loading quickly decays to zero as passive noise ($T \neq 0$, $\tau \rightarrow 0$) is added. In fact, the system is less robust to noise than the Hopfield model, for which patterns can be retrieved up to $T = 1$ [8, 9].

When the stability-enhancing term [second term of Eq. (1)] is turned on ($\epsilon > 0$, Fig. 2b), the retrievability of the learned patterns deteriorates less rapidly with temperature and pattern loading. In particular, retrieval is enabled at higher temperatures for which it does not occur when $\epsilon = 0$. These improvements come at the expense of being able to, at lower temperatures, also retrieve patterns that have not been learned (Fig. 2b, R_{L+NL} phase). For this reason, we restrict ourselves to $\epsilon \leq 1$ throughout this work.

Having characterized the system under passive noise, we now consider the system under active noise of equal strength (T) and with persistence time $\tau = 1$. Compared to passive noise, pattern retrieval is more resistant to pattern loading and noise strength (Fig. 3, a-b). Notably, retrieval is successful at noise strengths for which it fails under passive noise. The critical pattern loading at these noise strengths grows with ϵ (Fig. 3c). Similarly, for a given pattern loading, active noise raises the critical noise strength (i.e., the noise strength beyond which retrieval does not occur), and the relative increase scales with ϵ (Fig. 3d). These findings suggest that higher nonlinearity in the oscillator couplings allows active noise to better stabilize pattern configurations which are unstable under passive noise.

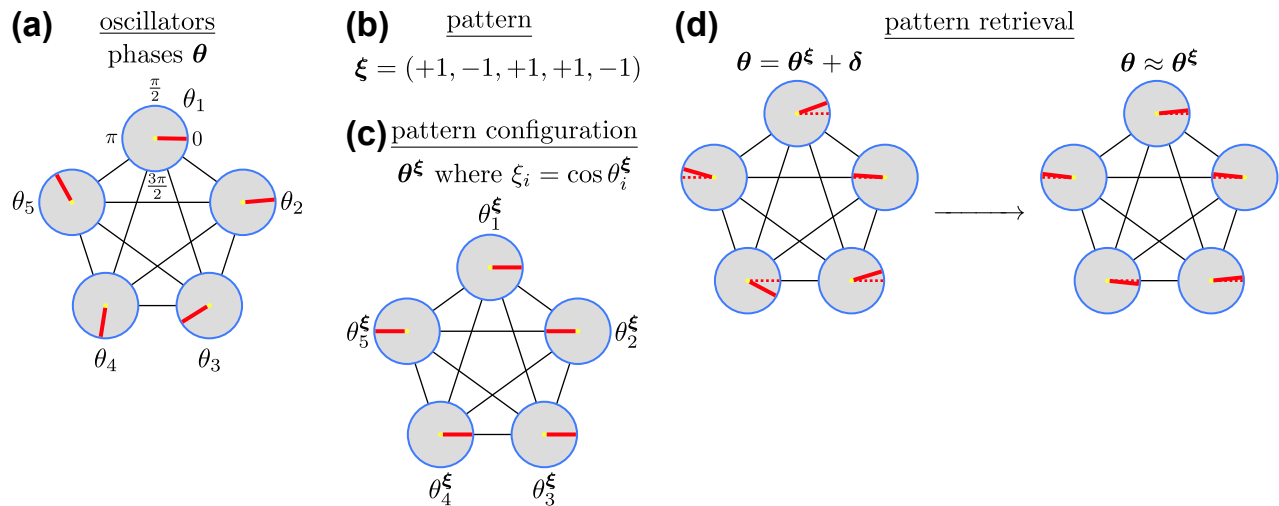


Figure 1. Oscillatory associative memory. (a) N coupled oscillators, represented as a graph whose vertices are the oscillator phases θ and the edges are the couplings. Here, $N = 5$. (b) A pattern, which is a vector $\xi \in \{\pm 1\}^N$. Here, $\xi = (+1, -1, +1, +1, -1)$. (c) A pattern configuration, which for pattern ξ is any θ^ξ such that $\cos \theta_i^\xi = \xi_i$. Here, $\theta^\xi = (0, \pi, 0, 0, \pi)$. (d) Pattern retrieval. The system starts slightly displaced from a target pattern ξ ($\theta = \theta^\xi + \delta$ for nonzero δ) and then approaches the pattern ($\theta \approx \theta^\xi$).

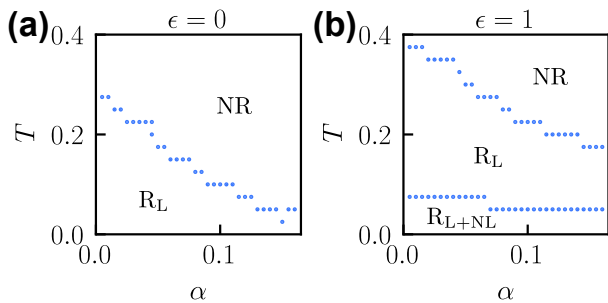


Figure 2. Retrieval phase diagram under passive noise, as calculated by simulation, for stability-enhancing coupling (a) $\epsilon = 0$ and (b) $\epsilon = 1$. In the retrieval phase R_{L+NL} , both learned and not-learned patterns can be retrieved (i.e., with final overlap > 0.8). In the retrieval phase R_L , only learned patterns can be retrieved. In the no retrieval (NR) phase, no patterns can be retrieved.

III. THEORY

To gain further insight on the improvement of memory due to active noise, we employ a perturbative expansion with respect to persistence time τ [23, 39]. This approach yields an effective equilibrium steady state, characterized by temperature T and a modified Hamiltonian. As we will show below, for the system studied here, the temporal correlations can be recast as an effective renormalization of coupling strengths. We then study the associated effective Hamiltonian using replica theory [42].

A. Effective equilibrium

Consider the steady-state probability distribution $P(\theta)$ of system configurations θ in the limit of small persistence time, $\tau \ll 1$. Following the method of either [23] or [39], we can write $P(\theta)$ in powers of τ and keep terms up to $O(\tau)$, yielding a Boltzmann-like distribution $P(\theta) \propto \exp(-H_{\text{eff}}/T)$, which is determined by an effective Hamiltonian with the general form [23]

$$H_{\text{eff}} = H + \tau \left(\frac{1}{2} |\nabla_{\theta} H|^2 - T \nabla_{\theta}^2 H \right). \quad (6)$$

Corresponding to an effective equilibrium steady state, this result can be alternatively obtained using the unified colored noise approximation [40, 41]. Plugging H [Eq. (1)] in the Laplacian term gives

$$\begin{aligned} H_{\text{eff}} = & -\frac{\zeta_1}{2N} \sum_{\mu=1}^p \sum_{i,j=1}^N \xi_i^\mu \xi_j^\mu \cos \theta_i \cos \theta_j \\ & -\frac{\zeta_2 \epsilon}{4N} \sum_{i,j=1}^N \cos 2\theta_i \cos 2\theta_j \\ & +\frac{\tau}{2} |\nabla_{\theta} H|^2 \\ & +\tau T \left\{ \frac{1}{N} \sum_{\mu=1}^p [\xi^\mu \cdot \mathbf{s}(\theta)]^2 + \frac{2\epsilon}{N} [\mathbf{1} \cdot \mathbf{s}(2\theta)]^2 \right\}, \quad (7) \end{aligned}$$

where $\zeta_1 = 1 + 2\tau T$, $\zeta_2 = 1 + 8\tau T$, and $\mathbf{s}(\theta) = (\sin \theta_1, \dots, \sin \theta_N)$. While it is possible to write $\frac{\tau}{2} |\nabla_{\theta} H|^2$ more explicitly in terms of θ , we have simply chosen not to do so, since the current expression is sufficient for physical interpretation (see below). Previously, we applied this small- τ expansion to the Hopfield model under

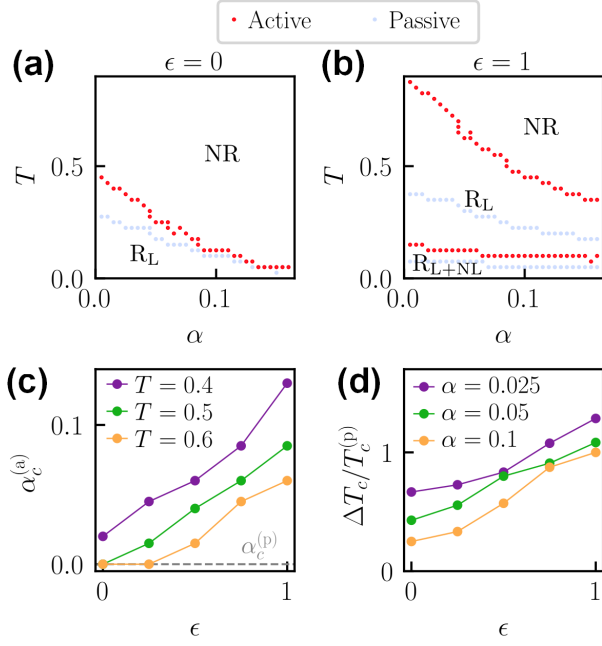


Figure 3. (a, b) Retrieval phase diagram under active noise ($\tau = 1$, red), as calculated by simulation, for stability-enhancing coupling (a) $\epsilon = 0$ and (b) $\epsilon = 1$. See the caption of Fig. 2 for a description of the various phases. For comparison, the transition lines under passive noise (reproduced from Fig. 2) are shown as blue translucent points. (c) Critical pattern loading (for the $R_L \rightarrow NR$ transition) under active noise ($\alpha_c^{(a)}$) as a function of ϵ . Results are shown for various noise strengths (T) at which patterns cannot be retrieved under passive noise (i.e., $\alpha_c^{(p)} = 0$, as indicated by gray dashed line). (d) Relative difference ($\Delta T_c / T_c^{(p)}$, where $\Delta T_c = T_c^{(a)} - T_c^{(p)}$) in the critical noise strength (for the $R_L \rightarrow NR$ transition) between active ($T_c^{(a)}$) and passive ($T_c^{(p)}$) noise as a function of ϵ . Results are shown for various pattern loadings (α).

active noise [44]. However, due to the constraint on the norm of the spin vector, we needed to make additional approximations to arrive at the effective Hamiltonian.

Note that the $\frac{\tau}{2} |\nabla_{\theta} H|^2$ term of H_{eff} [third line of Eq. (7)] is the squared norm of the (conservative) force ($-\nabla_{\theta} H$), which is zero at the energy minima near the patterns. Similarly, the fourth term of H_{eff} [fourth line of Eq. (7)] is zero at the patterns. Thus, these last two terms should play a minor role in pattern retrieval, which is determined by the energy landscape in the neighborhood of the patterns.

We therefore expect pattern retrieval under active noise to be approximately described by the effective

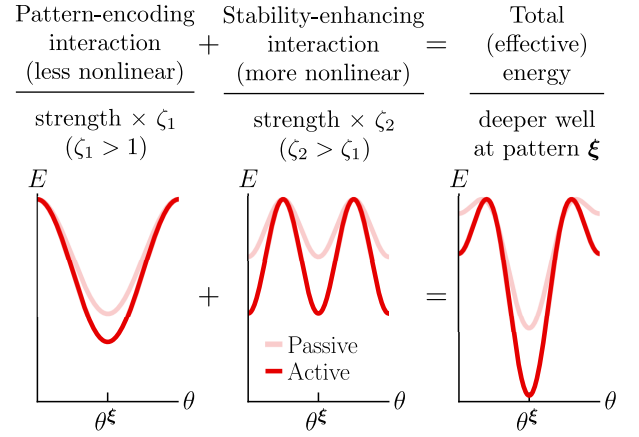


Figure 4. Schematic illustration of the mechanism, as described by effective Hamiltonian H_{eff} [Eq. (8)], by which active noise improves memory compared to passive noise. The temporal correlations of active noise effectively strengthen the oscillator interactions, where the more nonlinear interactions are preferentially enhanced. This strengthening leads to a deeper energy well at the patterns, and thus their retrieval becomes more robust to noise intensity and number of learned patterns.

Hamiltonian

$$H_{\text{eff}} = -\frac{\zeta_1}{2N} \sum_{\mu=1}^p \sum_{i,j=1}^N \xi_i^{\mu} \xi_j^{\mu} \cos \theta_i \cos \theta_j - \frac{\zeta_2 \epsilon}{4N} \sum_{i,j=1}^N \cos 2\theta_i \cos 2\theta_j, \quad (8)$$

which has the same form as the original Hamiltonian [Eq. (1)], except with the pattern-encoding term (first term) scaled by ζ_1 and the stability-enhancing term scaled by ζ_2 . Since $\zeta_1, \zeta_2 > 1$, active noise stabilizes the learned patterns (compared to passive noise) by deepening their respective energy wells. In particular, as implied by $\zeta_2 / \zeta_1 > 1$, the stability-enhancing term is amplified relative to the pattern-encoding term. More generally, the pattern-stabilizing interactions with more nonlinearity (i.e., the stability-enhancing term) are strengthened over those with less (i.e., the pattern-stabilizing term). This broader view suggests the importance of nonlinearity for memory under nonequilibrium settings. The impact of active noise on memory, as described by H_{eff} of Eq. (8), are summarized in Fig. 4. The limit of passive noise is recovered by setting $\tau = 0$, which yields the original Hamiltonian [Eq. (1)].

Note that the “active stabilization” described by H_{eff} of Eq. (8) arises from the $-\tau T \nabla_{\theta}^2 H$ term of the general form of H_{eff} [Eq. (6)] rather than the $\frac{\tau}{2} |\nabla_{\theta} H|^2$ term. The former energy correction, which depends on the curvature of the potential energy surface, has been shown to stabilize certain particle configurations in a related system, whose couplings go as the cosine of relative ori-

entations [39]. The result here stands in contrast to our previous work [44] on the continuous-spin Hopfield network of [45] under active noise: there, the interactions scale with the number $N \gg 1$ of spins in such a way that the $-\tau T \nabla_{\theta}^2 H$ term is negligible compared to the $\frac{\tau}{2} |\nabla_{\theta} H|^2$ term.

B. Replica calculation

Next, we apply replica theory [42] to the effective Hamiltonian H_{eff} of Eq. (8). Details of the calculation are presented in Appendix A. Replica theory allows one to calculate order parameters, such as the overlap with a pattern, of a system in the thermodynamic limit ($N \rightarrow \infty$) and averaged over randomly generated parameters of the Hamiltonian (known as “quenched disorder” in the literature [9]), such as the learned patterns. From the order parameters, one can determine what phase the system is in, e.g., ferromagnetic (retrieval) and spin glass (no retrieval). Following the convention of [8, 9, 11], a retrieval phase is defined by nonzero overlap with the target pattern (Section A 5). In contrast, our simulated results above (Figs. 2-3) use the criterion that the overlap exceeds 0.8 (caption of Fig. 2). Thus, our analysis below is limited to qualitative comparisons between the phase diagrams obtained by replica theory and simulation. Furthermore, our replica calculation is limited to $T > 0.1$; for $T \rightarrow 0$, we anticipate that the saddle-point equations [Eqs. (A19)-(A24)] which determine the order parameters can yield unstable solutions (Sec. A 3).

We first consider the system under passive noise, for which H_{eff} reduces to H [Eq. (1)], the original Hamiltonian. To our knowledge, H has not been previously studied using replica theory. Figs. 5a and 5b show the phase diagram calculated by this method for $\epsilon = 0$ and $\epsilon = 1$, respectively. Both plots qualitatively resemble the corresponding phase diagram for the Hopfield model [8, 9, 11]. At $T \lesssim 0.5$, increasing pattern loading induces transitions from the ferromagnetic retrieval phase (i.e., a global free energy minimum has significant overlap with the target pattern) to the mixed retrieval phase (i.e., the global minimum becomes a local minimum) to the spin glass phase, which does not support retrieval. The same phase transitions can be triggered by increasing T . At $T \gtrsim 0.5$, the target pattern cannot be retrieved at all; the system is in the paramagnetic phase at low pattern loading and the spin glass phase at high pattern loading.

Consistent with simulations (Fig. 2), replica theory (Fig. 5) reveals that the stability-enhancing term ($\epsilon > 0$) raises the critical temperature and pattern loading at which the system transitions from a retrieval (mixed) to a no-retrieval (spin glass) phase. Also increased are the critical values separating the two retrieval phases.

We proceed to the corresponding phase diagrams for the system under active noise. Since effective equilibrium theory is correct to $O(\tau)$ (Section III A), our application of replica theory to H_{eff} of Eq. (8) assumes

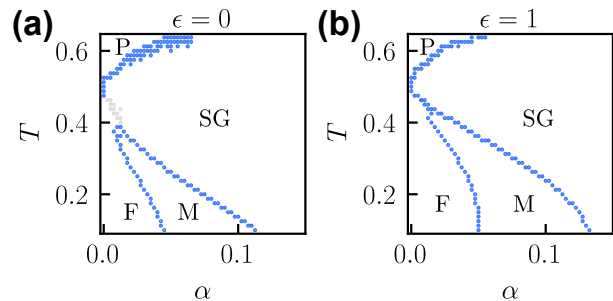


Figure 5. Retrieval phase diagram under passive noise, as calculated by theory, for stability-enhancing coupling (a) $\epsilon = 0$ and (b) $\epsilon = 1$. In the ferromagnetic (F) retrieval phase, the global minimum of free energy function f [Eq. (A15)] has nonzero overlap with the target pattern. In the mixed (M) retrieval phase, a local (but not global) minimum of f has nonzero overlap with the target pattern. No retrieval occurs in the spin glass (SG) and paramagnetic (P) phases, in which all minima of f have zero overlap with the target pattern. The gray points indicate where no minima of f could be found numerically (see Appendix A 4). Note that the plots start at $T = 0.1$, in contrast to the corresponding results from simulations (Fig. 2).

$\tau = 0.2$: this value is small enough for the theory to be a reasonable approximation but large enough to observe appreciable differences between active and passive noise. Fig. 6a-b shows phase diagrams obtained by the theory. Replacing passive with active noise enables the target pattern to be retrieved at higher noise strengths (for a given pattern loading) and pattern loadings (for a given noise strength). In addition, the relative increase in the critical noise strengths scales with ϵ (Fig. 6c). Remarkably, these features also appear in the simulated phase diagrams (Fig. 3, a-b, d) for $\tau = 1$, which falls outside the range of persistence times ($\tau \ll 1$) for which effective equilibrium theory is expected to be valid. This agreement suggests that H_{eff} of Eq. (8) can qualitatively describe how active noise improves memory, even for $\tau \geq 1$. As discussed in Section III A, the impact of active noise in this effective picture is to strengthen the interactions that stabilize the patterns, where the interactions with higher nonlinearity are enhanced over those with less. The replica calculation further reveals that active noise delays the transition (with respect to increasing noise strength and pattern loading) from the ferromagnetic retrieval phase to the mixed retrieval phase.

Before concluding, let us briefly discuss the quantitative aspects of the theory. In Appendix A 6, we evaluate how well the theory can reproduce the final overlap computed by simulations. For the case of passive noise, the agreement is semi-quantitative. For active noise, we observe similar agreement between the theory and simulations with the same persistence time ($\tau = 0.2$), though only at relatively low T . More details can be found in Appendix A 6.

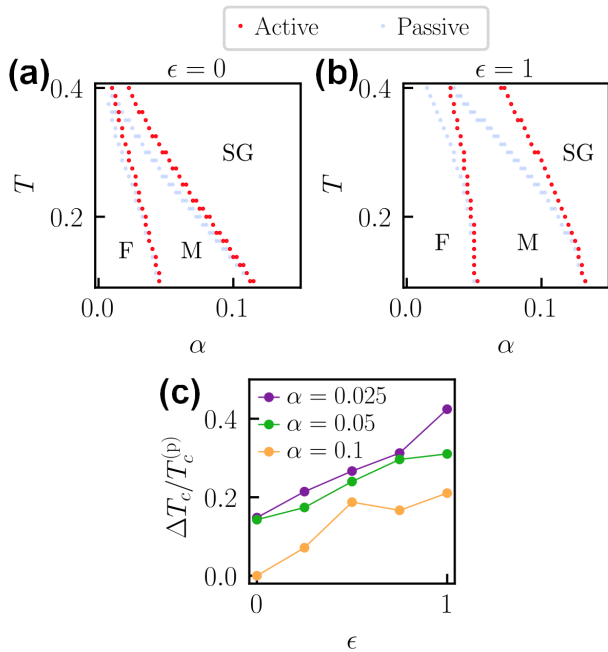


Figure 6. (a, b) Retrieval phase diagram under active noise ($\tau = 0.2$, red), as calculated by theory, for stability-enhancing coupling (a) $\epsilon = 0$ and (b) $\epsilon = 1$. The dotted lines indicate where phase transitions occur under passive noise (compare to corresponding panels of Fig. 5). See the caption of Fig. 5 for additional details. (c) Relative difference ($\Delta T_c / T_c^{(p)}$, where $\Delta T_c = T_c^{(a)} - T_c^{(p)}$) in the critical noise strength (for the $M \rightarrow SG$ transition) between active ($T_c^{(a)}$) and passive ($T_c^{(p)}$) noise, as calculated by theory and as a function of ϵ . Results are shown for various pattern loadings (α).

IV. CONCLUSION

We studied how active noise impacts periodic oscillators whose couplings endow the system with associative memory. One type of interaction encodes patterns, while the second type, a more nonlinear interaction, enhances the stability of the patterns. Through simulations, we showed that pattern retrieval under active noise is more robust to noise strength and number of learned patterns than under passive noise. This improvement in memory scales with the strength of the more nonlinear coupling relative to the less nonlinear coupling.

Using effective equilibrium theory, which is perturbative with respect to the persistence time of active noise, we analytically derived an effective Hamiltonian [Eq. (8)] that captures how the temporal correlations of active noise resculpt the potential energy landscape and thereby improve memory. Specifically, active noise leaves the oscillator interactions unchanged in form but increased in strength, with the more nonlinear interaction being preferentially enhanced. As a result of the stronger couplings, the energy basins at the pattern configurations become deeper. Unlike the Hopfield model studied in [44, 45], the

effect of active noise here arises mainly from the curvature of the original energy surface rather than the slope.

We then demonstrated qualitative agreement between this effective picture and the simulated results by applying replica theory to the effective Hamiltonian. This agreement is remarkable because effective equilibrium theory strictly holds for persistence time $\tau \ll 1$ while the simulations were run with $\tau = 1$. In addition, the replica analysis reveals that replacing passive with active noise can increase the critical noise strength at which a target pattern is converted from a global minimum of the (effective) free energy to a local minimum.

Overall, our findings highlight that having nonlinear couplings between neurons can be essential for associative memory under nonequilibrium conditions and thus biologically relevant contexts. For the Hopfield model in the absence of noise, highly nonlinear interactions have been shown to drastically increase the critical number of learned patterns beyond which the patterns can no longer be retrieved [46, 47]. Our study suggests that such nonlinearities may confer additional benefits to memory in noisy and nonequilibrium environments.

ACKNOWLEDGMENTS

M. D. and S. V. are supported by DOE BES Grant No. DE-SC0019765. A. K. B. is supported by a fellowship from the Department of Chemistry at the University of Chicago. We thank Carlos Floyd, David Martin, and Aditya Nandy for their feedback on earlier drafts of the manuscript.

Appendix A: Details of replica calculation

In this section, we apply replica theory [42] to effective Hamiltonian H_{eff} of Eq. (8). Our replica calculation largely follows those [8, 11] for the Hopfield Hamiltonian. Note that the first term of H_{eff} [Eq. (8)] has the same form as the Hamiltonian of the Hopfield model.

1. Gauge fixing

To simplify the calculation, we first choose a gauge for the patterns. Without loss of generality, we arbitrarily designate pattern 1 as the target pattern, $\xi \equiv \xi^1$, as we have done in our numerical simulations (Sec. II). We also apply an appropriate rotation to all memories such that $\xi = (1, \dots, 1)$. This transformation, which is orthogonal, does not change the final result of the calculation. Since we have fixed the target pattern, we only need to average over the other $p - 1$ patterns.

2. Replica theory

In replica theory [42], the free energy per oscillator— at (effective) equilibrium, averaged over the non-target patterns, and in the thermodynamic limit ($N \rightarrow \infty$)—is expressed in terms of a “replicated” partition function:

$$\lim_{N \rightarrow \infty} \frac{\overline{F}}{N} = - \lim_{N \rightarrow \infty} \frac{1}{\beta N} \overline{\ln Z} = - \lim_{N \rightarrow \infty} \lim_{n \rightarrow 0} \frac{1}{\beta N n} \ln \overline{Z^n}, \quad (\text{A1})$$

where $\overline{\dots}$ denotes the pattern average, $\beta = 1/T$ ($k_B = 1$) is the inverse temperature, $Z = \int d\boldsymbol{\theta} \exp[-\beta H_{\text{eff}}(\boldsymbol{\theta})]$ is the partition function, and n is the number of replicas of the system. Due to the periodicity of H_{eff} , the integral over each θ_i ($i = 1, \dots, N$) can be chosen to run over any (contiguous) interval of length 2π (e.g., $[0, 2\pi]$). Plugging in H_{eff} [Eq. (8)] of the chosen gauge, the replicated partition function can be written as

$$\begin{aligned} \overline{Z^n} &= \int d\overleftrightarrow{\boldsymbol{\theta}} \exp \left\{ \underbrace{\frac{\beta \zeta_1}{2N} \sum_{\gamma} [\boldsymbol{\xi} \cdot \mathbf{c}(\boldsymbol{\theta}^{\gamma})]^2}_{\equiv E_1} \right\} \\ &\times \exp \left\{ \underbrace{\frac{\beta \zeta_1}{2N} \sum_{\gamma} \sum_{\mu > 1} [\boldsymbol{\xi}^{\mu} \cdot \mathbf{c}(\boldsymbol{\theta}^{\gamma})]^2}_{\equiv E_2} \right\} \\ &\times \exp \left\{ \underbrace{\frac{\beta \zeta_2 \epsilon}{4N} \sum_{\gamma} [\mathbf{1} \cdot \mathbf{c}(2\boldsymbol{\theta}^{\gamma})]^2}_{\equiv E_3} \right\}, \quad (\text{A2}) \end{aligned}$$

where $\overleftrightarrow{\boldsymbol{\theta}} = (\boldsymbol{\theta}^1, \dots, \boldsymbol{\theta}^n)$ contains the configurations $\boldsymbol{\theta}^{\gamma} = (\theta_1^{\gamma}, \dots, \theta_N^{\gamma})$ of replica $\gamma = 1, \dots, n$. Note that E_2 includes the pattern average ($\overline{\dots}$). We next write each E_i as an integral, whose integration variables will become order parameters. The terms E_1 and E_2 are the contributions from the target pattern and non-target patterns, respectively. In analogy to the replica calculation for the Hopfield model [8, 11], we have

$$\begin{aligned} E_1 &= \left(\frac{N\beta\zeta_1}{2\pi} \right)^{n/2} \\ &\times \int d\mathbf{m} \exp \beta \zeta_1 \left\{ \sum_{\gamma} m^{\gamma} [\boldsymbol{\xi} \cdot \mathbf{c}(\boldsymbol{\theta}^{\gamma})] - \frac{N|\mathbf{m}|^2}{2} \right\}, \quad (\text{A3}) \end{aligned}$$

$$\begin{aligned} E_2 &= \left(\frac{N}{2\pi} \right)^{n^2} \\ &\times \int d\mathbf{q} d\hat{\mathbf{q}} \exp \left\{ i \sum_{\gamma\kappa} \hat{q}^{\gamma\kappa} [Nq^{\gamma\kappa} - \mathbf{c}(\boldsymbol{\theta}^{\gamma}) \cdot \mathbf{c}(\boldsymbol{\theta}^{\kappa})] \right\} \\ &\times [\det(\mathbf{I} - \beta\zeta_1\mathbf{q})]^{-p/2}, \quad (\text{A4}) \end{aligned}$$

where \mathbf{I} is the $n \times n$ identity matrix. In tensor notation, the integration variables are m^{γ} , $q^{\gamma\kappa}$, and $\hat{q}^{\gamma\kappa}$ for

$\gamma, \kappa = 1, \dots, n$. Note that Eq. (A4) has been written assuming $N \rightarrow \infty$ [8, 11]. The term E_3 is the contribution from the stability-enhancing term [second term of Eq. (1)]. Using a standard Gaussian integral identity, it is straightforward to show that

$$\begin{aligned} E_3 &= \left(\frac{N\beta\zeta_2\epsilon}{4\pi} \right)^{n/2} \\ &\times \int d\mathbf{w} \exp \frac{\beta\zeta_2\epsilon}{2} \left\{ \sum_{\gamma} w^{\gamma} [\mathbf{1} \cdot \mathbf{c}(2\boldsymbol{\theta}^{\gamma})] - \frac{N|\mathbf{w}|^2}{2} \right\}, \quad (\text{A5}) \end{aligned}$$

where the integration variables are (in tensor notation) w^{γ} for $\gamma = 1, \dots, n$. We can then substitute Eqs. (A3)-(A5) into Eq. (A2) and write the replicated partition function in the form $\overline{Z^n} = \int d\mathbf{m} d\mathbf{w} d\mathbf{q} d\hat{\mathbf{q}} \exp(\dots)$. Finally, we evaluate the free energy per oscillator [Eq. (A1)] using the saddle-point method,

$$\lim_{N \rightarrow \infty} \frac{\overline{F}}{N} = \min_{(\mathbf{m}, \mathbf{w}, \mathbf{q}, \hat{\mathbf{q}})} f(\mathbf{m}, \mathbf{w}, \mathbf{q}, \hat{\mathbf{q}}), \quad (\text{A6})$$

where

$$\begin{aligned} f(\mathbf{m}, \mathbf{w}, \mathbf{q}, \hat{\mathbf{q}}) &= \lim_{n \rightarrow 0} \frac{1}{\beta n} \left[\frac{\beta\zeta_1|\mathbf{m}|^2}{2} + \frac{\beta\zeta_2\epsilon|\mathbf{w}|^2}{4} \right. \\ &\quad \left. - i \sum_{\gamma\kappa} \hat{q}^{\gamma\kappa} q^{\gamma\kappa} + \frac{\alpha}{2} \ln \det(\mathbf{I} - \beta\zeta_1\mathbf{q}) \right. \\ &\quad \left. - \frac{1}{N} \ln \int d\overleftrightarrow{\boldsymbol{\theta}} G(\mathbf{m}, \mathbf{w}, \mathbf{q}, \hat{\mathbf{q}}, \overleftrightarrow{\boldsymbol{\theta}}) \right] \quad (\text{A7}) \end{aligned}$$

is the function to be minimized and

$$\begin{aligned} G(\mathbf{m}, \mathbf{w}, \mathbf{q}, \hat{\mathbf{q}}, \overleftrightarrow{\boldsymbol{\theta}}) &= \exp \left\{ \beta\zeta_1 \sum_{\gamma} m^{\gamma} [\boldsymbol{\xi} \cdot \mathbf{c}(\boldsymbol{\theta}^{\gamma})] \right. \\ &\quad \left. + \frac{\beta\zeta_2\epsilon}{2} \sum_{\gamma} w^{\gamma} [\mathbf{1} \cdot \mathbf{c}(2\boldsymbol{\theta}^{\gamma})] \right. \\ &\quad \left. - i \sum_{\gamma\kappa} \hat{q}^{\gamma\kappa} [\mathbf{c}(\boldsymbol{\theta}^{\gamma}) \cdot \mathbf{c}(\boldsymbol{\theta}^{\kappa})] \right\}. \quad (\text{A8}) \end{aligned}$$

As mentioned above, the independent variables of f correspond to order parameters. The parameter values that minimize f characterize the minima of the free energy landscape. In particular, the values that globally minimize f correspond to the (effective) equilibrium values and yield the (effective) equilibrium free energy through Eq. (A6).

The physical meaning of the order parameters can be deduced from the saddle-point equations. For example, the equations obtained by extremizing f [Eq. (A7)] with respect to m^{γ} and $\hat{q}^{\gamma\kappa}$ are

$$m^{\gamma} = \frac{1}{N} \langle \boldsymbol{\xi} \cdot \mathbf{c}(\boldsymbol{\theta}^{\gamma}) \rangle, \quad (\text{A9})$$

$$q^{\gamma\kappa} = \begin{cases} \frac{1}{N} \sum_{i=1}^N \langle \cos^2 \theta_i^{\gamma} \rangle, & \gamma = \kappa, \\ \frac{1}{N} \sum_{i=1}^N \langle \cos \theta_i^{\gamma} \cos \theta_i^{\kappa} \rangle, & \gamma \neq \kappa, \end{cases} \quad (\text{A10})$$

where we have defined the average $\langle h(\vec{\theta}) \rangle = \frac{\int d\vec{\theta} G(\vec{\theta}) h(\vec{\theta})}{\int d\vec{\theta} G(\vec{\theta})}$ for any function $h(\vec{\theta})$. As in the Hopfield model [8, 11], m^γ represents the overlap with the target memory (see Sec. I for definition of overlap), and $q^{\gamma\kappa}$ for $\gamma \neq \kappa$ is the Edwards-Anderson parameter [48] except with the variable of spin i replaced by $\cos\theta_i$. Thus, minimization of f will provide information about the overlap at free energy minima.

3. Replica-symmetric solution

To minimize f explicitly, we must impose some constraints on the values of the order parameters. Let us focus on the replica-symmetric ansatz

$$m^\gamma = m, \quad (\text{A11})$$

$$w^\gamma = w, \quad (\text{A12})$$

$$q^{\gamma\kappa} = Q\delta_{\gamma\kappa} + q(1 - \delta_{\gamma\kappa}), \quad (\text{A13})$$

$$\hat{q}^{\gamma\kappa} = \frac{i\alpha(\beta\zeta_1)^2}{2} [R\delta_{\gamma\kappa} + r(1 - \delta_{\gamma\kappa})]. \quad (\text{A14})$$

Then f [Eq. (A7)] reduces to

$$\begin{aligned} f(m, w, Q, q, R, r) = & \frac{\zeta_1 m^2}{2} + \frac{\zeta_2 \epsilon}{2} \left(\frac{w^2}{2} + w \right) \\ & + \frac{\alpha}{2} \left\{ \beta \zeta_1^2 (RQ - rq) \right. \\ & + \frac{1}{\beta} \ln [1 - \beta \zeta_1 (Q - q)] \\ & \left. - \frac{\zeta_1 q}{1 - \beta \zeta_1 (Q - q)} \right\} \\ & - \frac{1}{\beta} \int Dz \ln \mathcal{I}_0(m, w, R, r, z), \end{aligned} \quad (\text{A15})$$

where

$$\mathcal{I}_v(m, w, R, r, z) = \int d\theta g(m, w, R, r, \theta, z) \cos^v \theta, \quad (\text{A16})$$

$$\begin{aligned} g(m, w, R, r, \theta, z) = & \exp \beta \left\{ \zeta_1 (m + z\sqrt{\alpha r}) \cos \theta \right. \\ & \left. + \left[\zeta_2 \epsilon w + \frac{\alpha \beta \zeta_1^2}{2} (R - r) \right] \cos^2 \theta \right\}. \end{aligned} \quad (\text{A17})$$

In evaluating the determinant of Eq. (A7), we used the fact that \mathbf{q} is a $n \times n$ matrix of the form $M_{ij} = a\delta_{ij} + b(1 - \delta_{ij})$ and thus has eigenvalues $Q - q$ and $Q + (n - 1)q$ with multiplicities $n - 1$ and 1 , respectively. In addition, the integral in Eq. (A7) was simplified to that in Eq. (A15)

using the following facts: $\boldsymbol{\xi} = (1, \dots, 1)$, all oscillators are identical, all replicas are identical, and

$$\lim_{n \rightarrow 0} \frac{\ln \int Dz h^n(z)}{n} = \int Dz \ln h(z) \quad (\text{A18})$$

for any function h such that the limit can be evaluated using L'Hôpital's rule. The extrema of f are solutions of the saddle-point equations

$$m = \int Dz u_1(m, w, R, r, z), \quad (\text{A19})$$

$$w = -1 + 2Q, \quad (\text{A20})$$

$$Q = \int Dz u_2(m, w, R, r, z), \quad (\text{A21})$$

$$q = \int Dz u_1^2(m, w, R, r, z), \quad (\text{A22})$$

$$R = \frac{1}{\beta \zeta_1} \frac{1 - \beta \zeta_1 (Q - 2q)}{[1 - \beta \zeta_1 (Q - q)]^2}, \quad (\text{A23})$$

$$r = \frac{q}{[1 - \beta \zeta_1 (Q - q)]^2}, \quad (\text{A24})$$

where

$$u_v(m, w, R, r, z) = \frac{\mathcal{I}_v(m, w, R, r, z)}{\mathcal{I}_0(m, w, R, r, z)}. \quad (\text{A25})$$

Given that H_{eff} [Eq. (8)] is similar in form to the Hamiltonian of the Hopfield model [7], we expect the solution(s) of Eqs. (A19)-(A24) to eventually become unstable as $T \rightarrow 0$ for some values of α . Indeed, such instability in the replica-symmetric solution was found for the Hopfield model [8, 9, 11, 49]. This issue can be addressed by using an ansatz that breaks replica symmetry [42], which has been done for the Hopfield model [50, 51].

4. Numerical details

To numerically solve the saddle-point equations (A19)-(A24), we optimize with respect to m , Q , and q only, while w , Q , and q are constrained by Eqs. (A20), (A23), and (A24), respectively. The computation is done in Python using the `optimize.root` function (all keyword parameters take their default value, including `method='hybr'`) of the SciPy package. We repeat the calculation for initial conditions $(m, Q, q) = (0.9, 0.9, 0.9)$, $(0, 0.99, 0.9)$, $(0, 0.9, 0.9)$, $(0, 0.8, 0.6)$, $(0, 0.6, 0)$, $(0, 0.4, 0.1)$, $(0, 0.49999999, 0)$. We accept solutions (m, Q, q) for which the maximum relative error, with respect to the nonzero elements, is less than 10^{-6} . For each order parameter $x = m, Q, q$, the relative error is calculated as $(x_{\text{solution}} - x_{\text{actual}})/x_{\text{solution}}$, where x_{solution} is the value in the solution and x_{actual} is the value computed from the right-hand side of the saddle-point equation for x . We note that, for some choices of model parameters $(\alpha, \epsilon, T, \tau)$, no solution could be found using the attempted initial conditions.

5. Determination of phases

For a given choice of model parameters $(\alpha, \epsilon, T, \tau)$, we assign a phase according to the sets of order parameters that solve saddle-point equations (A19)-(A24) and thus extremize f [Eq. (A15)]. Specifically, the phase is determined by (m, q) of the global minimum of f and m of the local minima, as done in replica calculations of the Hopfield model [8, 9, 11] and reviewed in Table I. The existence of a local minimum with $m \neq 0$ implies that the target pattern can be retrieved, while the absence thereof implies that retrieval is not possible.

6. Calculation of overlap: theory versus simulation

The highest overlap, with respect to all minima of f , is expected to correspond to the final overlap in a simulation of pattern retrieval. Fig. 7 compares the highest overlap calculated in our theory (lines) with the final overlap obtained in our simulations (circles).

We first focus on the system under passive noise (Fig. 7, blue). Quantitative agreement is obtained at low pattern loading, while the theoretical overlap reasonably ap-

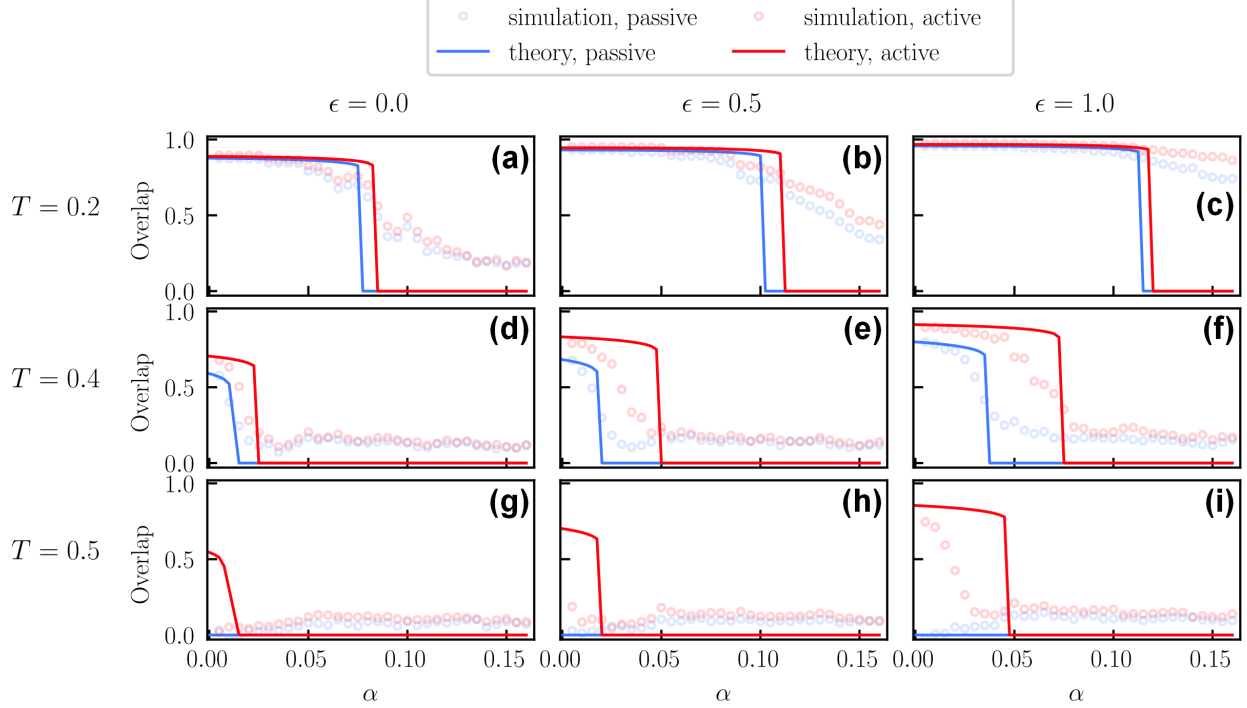
proximates the decay of the simulated overlap as the pattern loading increases. Note, however, that the theory overestimates the overlap during the decay and incorrectly predicts that the overlap approaches zero. We attribute these discrepancies to the fact that the simulations are done for a finite number N of oscillators while the theory assumes $N \rightarrow \infty$.

Having validated the theory for the case of passive noise, we now turn to the system under active noise with $\tau = 0.2$ (Fig. 7, red). Like the case of passive noise, we see good agreement between simulation and theory at relatively low pattern loading and noise strength. In contrast, at sufficiently high noise strength, the theory predicts significant overlap under active noise while the simulations show little overlap (Figs. 7g-7h). We believe this discrepancy is related to the following: the effective Hamiltonian [Eq. (8)] used in the replica calculation does not include the $\frac{\tau}{2} |\nabla_{\theta} H|^2$ term of the full effective Hamiltonian [Eq. (6)] derived by effective equilibrium theory (Section III A). At higher noise strengths, the system is kicked away from the patterns, and so $-\nabla_{\theta} H$, the force pushing the system towards the patterns, becomes significant.

-
- [1] N. C. Keim, J. D. Paulsen, Z. Zeravcic, S. Sastry, and S. R. Nagel, *Reviews of Modern Physics* **91**, 035002 (2019).
- [2] A. S. Sokolov, H. Abbas, Y. Abbas, and C. Choi, *Journal of Semiconductors* **42**, 013101 (2021).
- [3] D. J. Amit, *Modeling brain function: The world of attractor neural networks* (Cambridge university press, 1989).
- [4] K. Nakano, *IEEE Transactions on Systems, Man, and Cybernetics SMC-2*, 380 (1972).
- [5] T. Kohonen, *IEEE Transactions on Computers* **C-21**, 353 (1972).
- [6] S.-I. Amari, *IEEE Transactions on Computers* **C-21**, 1197 (1972).
- [7] J. J. Hopfield, *Proceedings of the National Academy of Sciences* **79**, 2554 (1982).
- [8] D. J. Amit, H. Gutfreund, and H. Sompolinsky, *Annals of Physics* **173**, 30 (1987).
- [9] D. J. Amit, H. Gutfreund, and H. Sompolinsky, *Physical Review Letters* **55**, 1530 (1985).
- [10] M. V. Feigelman and L. B. Ioffe, *Europhysics Letters* **1**, 197 (1986).
- [11] A. C. C. Coolen, in *Handbook of Biological Physics*, Neuro-Informatics and Neural Modelling, Vol. 4, edited by F. Moss and S. Gielen (North-Holland, 2001) pp. 553–618.
- [12] F. S. Gnesotto, F. Mura, J. Gladrow, and C. P. Broedersz, *Reports on Progress in Physics* **81**, 066601 (2018).
- [13] X. Fang, K. Kruse, T. Lu, and J. Wang, *Reviews of Modern Physics* **91**, 045004 (2019).
- [14] T. Vicsek, A. Czirók, E. Ben-Jacob, I. Cohen, and O. Shochet, *Physical Review Letters* **75**, 1226 (1995).
- [15] J. Toner, Y. Tu, and S. Ramaswamy, *Annals of Physics Special Issue*, **318**, 170 (2005).
- [16] F. Jülicher, K. Kruse, J. Prost, and J. F. Joanny, *Physics Reports* **449**, 3 (2007).
- [17] S. Banerjee, M. L. Gardel, and U. S. Schwarz, *Annual Review of Condensed Matter Physics* **11**, 421 (2020).
- [18] S. Ramaswamy, *Annual Review of Condensed Matter Physics* **1**, 323 (2010).
- [19] M. C. Marchetti, J. F. Joanny, S. Ramaswamy, T. B. Liverpool, J. Prost, M. Rao, and R. A. Simha, *Reviews of Modern Physics* **85**, 1143 (2013).
- [20] C. Bechinger, R. Di Leonardo, H. Löwen, C. Reichhardt, G. Volpe, and G. Volpe, *Reviews of Modern Physics* **88**, 045006 (2016).
- [21] N. Sepúlveda, L. Petitjean, O. Cochet, E. Grasland-Mongrain, P. Silberzan, and V. Hakim, *PLOS Computational Biology* **9**, e1002944 (2013).
- [22] C. Maggi, M. Paoluzzi, N. Pellicciotta, A. Lepore, L. Angelani, and R. Di Leonardo, *Physical Review Letters* **113**, 238303 (2014).
- [23] E. Fodor, C. Nardini, M. E. Cates, J. Tailleur, P. Visco, and F. van Wijland, *Physical Review Letters* **117**, 038103 (2016).
- [24] D. Martin, J. O’Byrne, M. E. Cates, E. Fodor, C. Nardini, J. Tailleur, and F. van Wijland, *Physical Review E* **103**, 032607 (2021).
- [25] M. J. Chacron, A. Longtin, M. St-Hilaire, and L. Maler, *Physical Review Letters* **85**, 1576 (2000).
- [26] N. Fourcaud and N. Brunel, *Neural Computation* **14**, 2057 (2002).
- [27] A. I. Selverston and M. Moulins, *Annual Review of Physiology* **47**, 29 (1985).
- [28] L. M. Ward, *Trends in Cognitive Sciences* **7**, 553 (2003).
- [29] X.-J. Wang, *Physiological reviews* **90**, 1195 (2010).
- [30] H. G. Schuster and P. Wagner, *Biological Cybernetics*

Phase	Retrieval or no retrieval of target pattern?	(m, q) of the global minimum of f	m of the local minima (if any) of f
ferromagnetic (F)	retrieval	$m \neq 0, q \neq 0$	$m = \text{any value}$
mixed (M)	retrieval	$m = 0, q \neq 0$	$m \neq 0$ for ≥ 1 minimum
spin glass (SG)	no retrieval	$m = 0, q \neq 0$	$m = 0$ for all minima
paramagnetic (P)	no retrieval	$m = 0, q = 0$	$m = 0$ for all minima

Table I. Phases of Hopfield-like models as described within replica theory.

Figure 7. Overlap with target pattern versus pattern loading α , as calculated by simulation (circles) and theory (lines). Results are shown for passive (purple) and active (blue, $\tau = 0.2$) noise; noise strength (a-c) $T = 0.2$, (d-f) $T = 0.4$, and (g-i) $T = 0.5$; and stability-enhancing coupling (a, d, g) $\epsilon = 0$, (b, e, h) $\epsilon = 0.5$, and (c, f, i) $\epsilon = 1$.

- 64, 77 (1990).
- [31] A. Arenas and C. J. P. Vicente, *Europhysics Letters* **26**, 79 (1994).
- [32] T. Fukai and M. Shiino, *Europhysics Letters* **26**, 647 (1994).
- [33] T. Fukai, *Biological Cybernetics* **70**, 427 (1994).
- [34] K. Park and M. Y. Choi, *Physical Review E* **52**, 2907 (1995).
- [35] T. Aonishi, *Physical Review E* **58**, 4865 (1998).
- [36] T. Aoyagi and K. Kitano, *Neural computation* **10**, 1527 (1998).
- [37] Y. Kuramoto, in *International Symposium on Mathematical Problems in Theoretical Physics: January 23-29, 1975, Kyoto University, Kyoto/Japan* (Springer, 1975) pp. 420–422.
- [38] T. Nishikawa, Y.-C. Lai, and F. C. Hoppensteadt, *Physical Review Letters* **92**, 108101 (2004).
- [39] A. Maitra and R. Voituriez, *Physical Review Letters* **124**, 048003 (2020).
- [40] P. Jung and P. Hänggi, *Physical Review A* **35**, 4464 (1987).
- [41] C. Maggi, U. M. B. Marconi, N. Gnan, and R. Di Leonardo, *Scientific Reports* **5**, 10742 (2015).
- [42] M. Mézard, G. Parisi, and M. A. Virasoro, *Spin glass theory and beyond: An Introduction to the Replica Method and Its Applications*, Vol. 9 (World Scientific Publishing Company, 1987).
- [43] D. O. Hebb, *The organization of behavior: A neuropsychological theory* (Psychology press, 2005).
- [44] A. K. Behera, M. Rao, S. Sastry, and S. Vaikuntanathan, [arXiv:2203.03024](https://arxiv.org/abs/2203.03024) (2022).
- [45] D. Bollé, T. M. Nieuwenhuizen, I. P. Castillo, and T. Verbeiren, *Journal of Physics A: Mathematical and General* **36**, 10269 (2003).
- [46] D. Krotov and J. J. Hopfield, in *Advances in Neural Information Processing Systems*, Vol. 29 (Curran Associates, Inc., 2016).
- [47] H. Ramsauer, B. Schäfl, J. Lehner, P. Seidl, M. Widrich, T. Adler, L. Gruber, M. Holzleitner, M. Pavlović, G. K. Sandve, V. Greiff, D. Kreil, M. Kopp, G. Klambauer,

- J. Brandstetter, and S. Hochreiter, [Hopfield Networks is All You Need](#) (2021).
- [48] S. F. Edwards and P. W. Anderson, [Journal of Physics F: Metal Physics](#) **5**, 965 (1975).
- [49] J.-P. Naef and A. Canning, [Journal de Physique I](#) **2**, 247 (1992).
- [50] A. Crisanti, D. J. Amit, and H. Gutfreund, [Europhysics Letters](#) **2**, 337 (1986).
- [51] H. Steffan and R. Kühn, [Zeitschrift für Physik B Condensed Matter](#) **95**, 249 (1994).